Measurements of the weak bonding interfacial stiffness by using air-coupled ultrasound

Cite as: AIP Advances **7**, 125316 (2017); https://doi.org/10.1063/1.5001248
Submitted: 23 August 2017 • Accepted: 06 December 2017 • Published Online: 14 December 2017

Wen-Lin Wu, Xing-Guo Wang, Zhi-Cheng Huang, et al.

Measurements of the weak bonding interfacial stiffness by using air-coupled ultrasound

Wen-Lin Wu, Xing-Guo Wang,[a] Zhi-Cheng Huang, and Nan-Xing Wu
School of Mechanical and Electronic Engineering, Jingdezhen Ceramic Institute, Jingdezhen 333403, China

(Received 23 August 2017; accepted 6 December 2017; published online 14 December 2017)

An air-coupled ultrasonic method, focusing on the problem that weak bonding interface is difficult to accurately measure using conventional nondestructive testing technique, is proposed to evaluate the bond integrity. Based on the spring model and the potential function theory, a theoretical model is established to predict the through-transmission spectrum in double-layer adhesive structure. The result of a theoretical algorithm shows that all the resonant transmission peaks move towards higher frequency with the increase of the interfacial stiffness. The reason for these movements is related to either the normal stiffness (K_N) or the transverse stiffness (K_T). A method to optimize the measurement parameters (i.e. the incident angle and testing frequency) is put forward through analyzing the relationship between the resonant transmission peaks and the interfacial spring stiffness at the frequency below 1MHz. The air-coupled ultrasonic testing experiments at the normal and oblique incident angle respectively are carried out to verify the theoretical analysis and to accurately measure the interfacial stiffness of double-layer adhesive composite plate. The experimental results are good agreement with the results from the theoretical algorithm, and the relationship between bonding time and interfacial stiffness is presented at the end of this paper. https://doi.org/10.1063/1.5001248

I. INTRODUCTION

Adhesively bonding is increasingly used in automotive and aerospace industries, as it has reliably sealing performance and excellent shock absorption capacity compared with welding and bolting.[1,2] However, manufacturing imperfections viz., weak bonding, micro-porosity and micro-cracks, etc. cause some serious accidences frequently. These imperfections, especially for weak bonding interface, are complicated to implement using conventional non-destructive testing (NDT) techniques, and restrict the application of bonding technology to some extent.[3–5] A large amount of NDT methods have been proposed on inspection of bond interfacial integrity for decades.[6–9]

Unfortunately, there is not any perfect method to evaluate this integrity. Dielectric technique has been used to measure carbon fiber reinforced plastic bonded structures by Boinard et al.,[10] but it is low resolution to local defects on large structures. Laser ultrasonic system is not only expensive, but harmful for operational staffs who do not take safety precautions.[11] Yang Zhengwei, et al. proposed that the infrared thermography method can be employed to estimate the defect of adhesive structure,[12] whereas this method is not suitable for weak bonding structures. Eddy currents methods only for conducting materials are limited by the tested material.

The past several years have witnessed the thriving of ultrasonic evaluation techniques, especially, which have been applied to detect adhesive bonding quality,[13–18] but so far there are many demerits for these techniques. Lamb waves, which are enable to assess a long length of adhesive for a single

[a]Corresponding author. E-mail: wangxingguo@jci.edu.cn

measurement, have lower accuracy than bulk waves in terms of the measurement adhesive interface integrity on a certain point.[19–21] Pulse-echo method is unfitted when the thickness of the adhesive layer is small, since reflection echoes from the rear adhesive interface interference with one from the front adhesive interface.[22,23] Reflection spectra method proposed by Paralusz[24] has limited application because the acoustic impedance of the upper layer is approximately the same as that of the lower layer. As a result, the reflected signal from the interface of the double layer is too weak. All of the above reasons cause inconvenient to detect using ultrasonic technique.

Compared with traditional ultrasonic techniques (i.e. contact and immersion ultrasonic technique), an air-coupled ultrasonic technique does not pollute the material surface and is appropriate for the materials which could be damaged by immersing the liquid. This technique has the potentiality for detecting the bonded quality of the producing line due to convenient installation and high testing efficiency. However the air-couple ultrasound has some drawbacks such as narrow bandwidth, low signal-to-noise ratio and low resolution.[25,26] Furthermore, it is only suitable for utilizing low frequency since the ultrasonic attenuation in air sharply increases with the increasing of the basic frequency.[27]

A considerable amount of efforts have been made to inspect adhesive bond integrity by using the air-couple ultrasonic technique,[27–29] but few attempts have been made in improving the inspection accuracy. In this paper testing parameters of interfacial stiffness have been optimized by the theoretical analysis at frequency below 1MHz. During the experiment, some double-layer composite specimens have been prepared using a two part epoxy adhesive. These specimens have obviously different bonding strength depend on the different bonding time. Subsequently, normal and transverse interfacial stiffness have been measured using the method of combining normal and oblique incidence.

II. THEORY

A. Physical models of air-coupled ultrasonic measurements

Figure 1 shows the physical model for the detection of weak bonding interface using oblique incidence air-coupled ultrasound. Ultrasound is emitted through transducer at the surface of tested materials with an angle of θ_i. Parts of them reflected from the air-solid interface with an angle of θ_r, and the others transferred into longitudinal wave and shear wave transmit into the composite material 1. The propagation of ultrasound in the tested materials is omitted for concise. Finally, the ultrasonic signal transits from the tested materials into the air with an angle of θ_t.

As shown in Fig. 1, the tested material is consisted of the composite material 1 (density ρ_1, thickness d_1, Lamé constants λ_1 and μ_1) and the composite material 2 (density ρ_2, thickness d_2, Lamé constants λ_2 and μ_2), which are held together by adhesive layer. Due to the thickness of the adhesive layer is less than 0.1mm, the properties of adhesive layer are negligible and are substituted for the spring model proposed by Newmark N M, et al.[30] K_N and K_T are the normal stiffness and transverse stiffness, respectively. x and z denote coordinate axis, and the direction of the x-axis and z-axis is right and down, respectively.

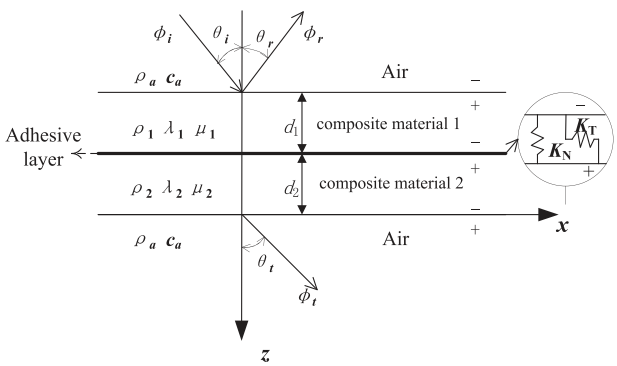

FIG. 1. Schematic diagram of oblique incidence air-coupled ultrasonic inspection.

B. Mathematical models

Currently, the common method to analyze the principle of ultrasonic wave propagation in multi-layer material structures is the transfer matrix model.[31] This model is convenient when there are a great amount of layers in the structures. But there are some issues of numerical instability when frequency-thickness products are large. To investigate the transmission coefficient of the double adhesive layers described by 1.1 section, a global matrix, which includes the quantitative relationship between the stresses and displacements on every interface, is more suitable. This matrix is established as follows.

The potential function of longitudinal waves and shear waves in the composite materials are expressed as shown below.[31]

$$\begin{aligned}\phi_{(m)} &= (\phi_{i(m)}e^{-\mathrm{i}\,k_{L(m)}\cos\theta_{L(m)}z} + \phi_{r(m)}e^{\mathrm{i}\,k_{L(m)}\cos\theta_{L(m)}z})E \\ \psi_{(m)} &= (\psi_{i(m)}e^{-\mathrm{i}\,k_{T(m)}\cos\theta_{T(m)}z} + \psi_{r(m)}e^{\mathrm{i}\,k_{T(m)}\cos\theta_{T(m)}z})E\end{aligned}, \tag{1}$$

Where Φ and Ψ are the longitudinal wave and shear wave potential functions respectively. Hereafter the symbols with a subscript (m) represent the corresponding parameters of composite material m (m=1 or 2), and the symbols with subscript L and T are the parameters of longitudinal wave and shear wave respectively. Φ_i and Φ_r are the incidence and reflection amplitude of the longitudinal wave potential function, and Ψ_i and Ψ_r are the incidence and reflected amplitude of the shear wave potential function, respectively. k is the wave number, and θ_{i} is the angle of the acoustic wave in the composite material. E=$e^{\mathrm{i}(\xi x-\omega t)}$ where ω is the circular frequency. ξ is the wave number in the x-direction. The wave number can be expressed by Snell' law as follow

$$\xi = k_L \sin\theta_i = k_{L(m)} \sin\theta_{L(m)} = k_{T(m)} \sin\theta_{T(m)}. \tag{2}$$

Since there is only longitudinal wave in the air, the potential function of acoustic wave in the top and bottom air are expressed, respectively

$$\begin{aligned}\phi_{(t)} &= (e^{-\mathrm{i}k_a\cos\theta_i z} + Re^{\mathrm{i}k_a\cos\theta_r z})E \\ \phi_{(b)} &= Te^{-\mathrm{i}k_a\cos\theta_t z}E\end{aligned}. \tag{3}$$

Hereafter, symbols with a subscript (t) and (b) are the corresponding parameters of upper and below air layer respectively. k_a is the wave number in the air. R and T are the reflection and transmission coefficient, respectively. The normal and tangential displacement and stress (u_x, u_z, σ_x and σ_z) can be calculated as shown in Eq. (4)

$$\begin{aligned}u_x &= \frac{\partial\phi}{\partial x} - \frac{\partial\psi}{\partial z} \\ u_z &= \frac{\partial\phi}{\partial z} + \frac{\partial\psi}{\partial x} \\ \sigma_z &= \lambda\frac{\partial u_x}{\partial x} + (\lambda+2\mu)\frac{\partial u_z}{\partial z} \\ \sigma_x &= \mu\left(\frac{\partial u_x}{\partial z} + \frac{\partial u_z}{\partial x}\right)\end{aligned}. \tag{4}$$

These boundary conditions of the air-solid interface are mathematically described as

$$\begin{aligned} u^-_{z(t)} &= u^+_{z(1)} & \qquad u^+_{z(b)} &= u^-_{z(2)} \\ \sigma^-_{z(t)} &= \sigma^+_{z(1)} & \qquad \sigma^+_{z(b)} &= \sigma^-_{z(2)} \\ \sigma^-_{x(t)} &= \sigma^+_{x(1)} = 0 & \qquad \sigma^+_{x(b)} &= \sigma^-_{x(2)} = 0 \end{aligned}. \tag{5}$$

The symbol with superscript – and + denotes the parameters at a certain layer of top and bottom respectively. The boundary condition of the adhesive layer is given by the spring model

$$\begin{aligned}\sigma^-_{x(2)} &= K_T(u^-_{x(1)} - u^+_{x(2)}) \\ \sigma^-_{z(2)} &= K_N(u^-_{z(1)} - u^+_{z(2)}) \\ \sigma^-_{x(1)} &= \sigma^+_{x(2)} \\ \sigma^-_{z(1)} &= \sigma^+_{z(2)}\end{aligned}. \tag{6}$$

According to Eq. (5) and Eq. (6). Ten equations could be obtained and rewrite them into a matrix form.

$$\begin{bmatrix} A_{11} & A_{12} & \cdots & A_{1(10)} \\ A_{21} & A_{22} & \cdots & A_{2(10)} \\ \vdots & \vdots & \ddots & \vdots \\ A_{(10)1} & A_{(10)2} & \cdots & A_{(10)(10)} \end{bmatrix} \begin{bmatrix} R \\ \phi_{i(1)} \\ \phi_{r(1)} \\ \psi_{i(1)} \\ \psi_{r(1)} \\ \phi_{i(2)} \\ \phi_{r(2)} \\ \psi_{i(2)} \\ \psi_{r(2)} \\ T \end{bmatrix} = \begin{bmatrix} -k_a \cos\theta_i \\ -\rho_a \omega^2 \\ 0 \\ 0 \\ 0 \\ 0 \\ 0 \\ 0 \\ 0 \\ 0 \end{bmatrix}, \tag{7}$$

The elements of matrix A are given in the Appendix.

III. NUMERICAL CALCULATION

In the case of knowing the physical parameters of the composite materials which are linear elastic isotropic materials, the reflection coefficient and transmission coefficient could be calculated by solving Eq. (7). Lamé constants λ and μ can be obtained using Eq. (8). The other parameters are provided by the manufacturer and listed in Table I.

$$\begin{aligned} \lambda &= \rho({c_L}^2 - 2{c_T}^2) \\ \mu &= \rho {c_T}^2 \end{aligned}. \tag{8}$$

Figure 2 shows distribution of the transmission coefficient T, along the frequency f and the incident angle θ_i under different conditions of the interfacial stiffness. The situation K_T=1×10^{20} N·m^{-3} and K_N=1×10^{20} N·m^{-3} (perfect interface) have been given in Fig. 2(a), K_T=1×10^{12} N·m^{-3} and K_N=1×10^{20} N·m^{-3} (transverse weak interface) in Fig. 2(b), K_T=0 N·m^{-3} and K_N=1×10^{20} N·m^{-3} (sliding interface) in Fig. 2(c), K_T=1×10^{20} N·m^{-3} and K_N=1×10^{14} N·m^{-3} (normal weak interface) in Fig. 2(d), K_T=1×10^{20} N·m^{-3} and K_N=0 N·m^{-3} (normal weak interface) in Fig. 2(e).

The changing rules of transmission peaks are shown in Fig. 2(a), Fig. 2(b) and Fig. 2(c), as the normal stiffness K_N remains constant and the transverse stiffness K_T varies from 1×10^{20} N·m^{-3} to 0. The boundary condition, K_T is 0 and K_N is 1×10^{20} N·m^{-3}, can be viewed as the situation that between the two adhesive bodies, there is a layer of infinite thin and cohesionless liquid which transfer only normal stress, but no tangential stress.[32] In order to describe these rules conveniently, these curves as shown in Fig. 2 have been labeled 'A_n' and 'B_n' (n=1, 2, 3, 4). It can be observed that the curve labeled 'A_n' remain the same in all figures, but the curve labeled 'B_n' change a lot. It is demonstrated that some of transmission peaks do not change when the value of K_T change from 0 to 1×10^{20} N·m^{-3}and the others do.

Based on the model of above researches, the change rule of transmission peaks can be analyzed by comparing Fig. 2(a), Fig. 2(d) and Fig. 2(e), when the value of K_T remains constant and the value of K_N varies from 1×10^{20} N·m^{-3} to 0. (note: the boundary conditions in Fig. 2(d) and Fig. 2(e) are extremely rare in reality. Researching these situation are only for finding the change rules). The results indicate the curve labeled 'A_n' can be influenced by the K_N, and the curve labeled 'B_n' can be not. Therefore, parts of the transmission peaks only depend on the normal stiffness (K_N) and others only

TABLE I. Physical parameters of the materials.

Material	P-wave velocity /(m/s)	S-wave velocity /(m/s)	Density /(kg/m^3)	Thickness /mm
Air	340	N/A	1	N/A
Composite material	2710	1220	1200	4.7
Composite material	2710	1220	1200	4.7

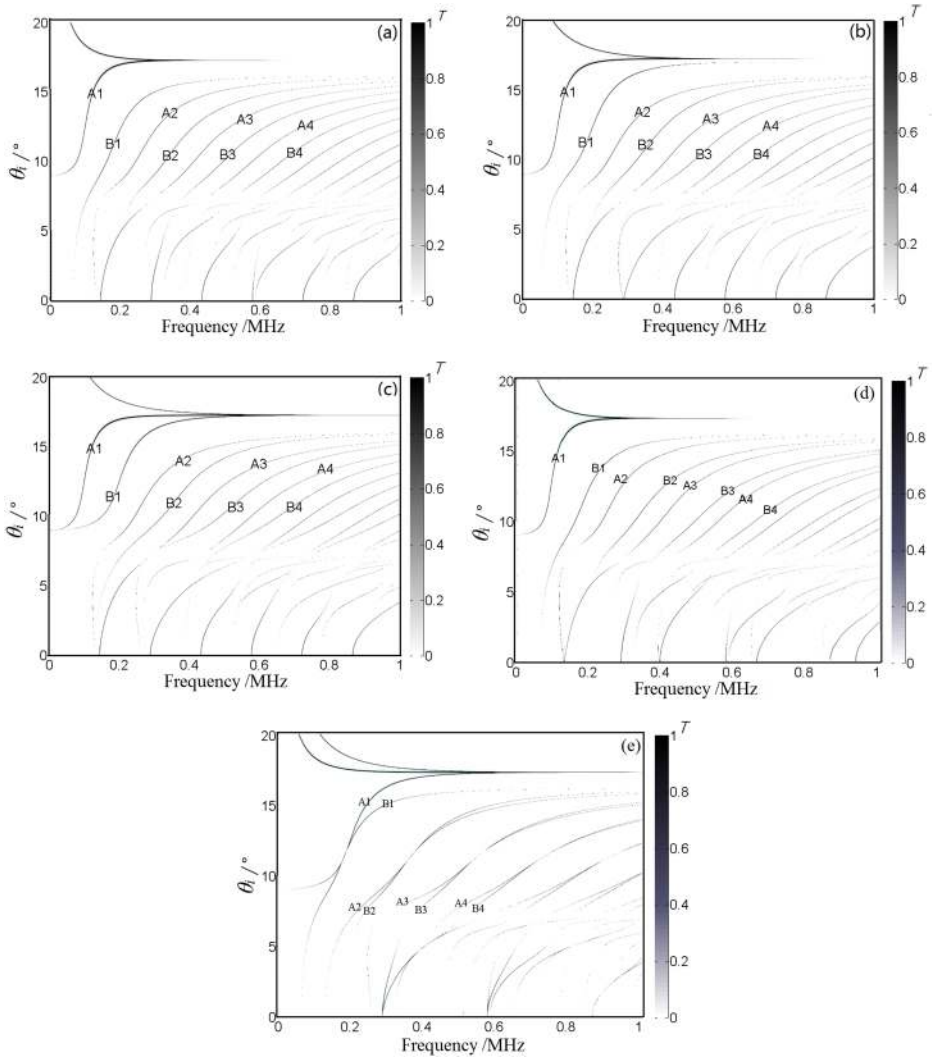

FIG. 2. Distribution of the transmission coefficient along the frequency and incident angle ((a) K_T=1×10^{20}N·m^{-3}, K_N=1×10^{20}N·m^{-3}; (b) K_T=1×10^{12}N·m^{-3}, K_N=1×10^{20}N·m^{-3}; (c) K_T=0 N·m^{-3}, K_N=1×10^{20}N·m^{-3}; (d) K_T=1×10^{20} N·m^{-3}, K_N=1×10^{14} N·m^{-3}; (e) K_T=1×10^{20} N·m^{-3}, K_N=0 N·m^{-3}).

depend on the transverse stiffness (K_T). Researching these correlations can contribute to measuring the stiffness K_N and K_T.

Under the condition of the angle of incidence less than 8°, namely the first critical angle, there are a large amount of resonant peaks. The amplitude of these peaks is slight, so they probably mislead us. However, as the incident angle is more than 15°, there are hardly any resonant peaks. In summary, the incident angles, from 8° to 15°, are not considered to measure the stiffness.

A. Optimization of the parameters for measuring the normal stiffness

It is crucial to confirm the optimal measurement parameters viz., the angle of incidence and the basic frequency, for inspection of weak bond interface according to these correlations. The normal incidence ultrasonic inspection has been extensively used to detect the normal stiffness K_N.[33] In the case of normal incidence, the transmission spectra do not change even if the transverse stiffness K_T varies all the time. That is because there is only the normal stresses in the tested materials at the incident angle zero degree.

Figure 3 shows the shift of the transmission peaks with respect to the normal stiffness at different frequency, when the incident angle is zero degree. From the figure, that parts of these peaks shift

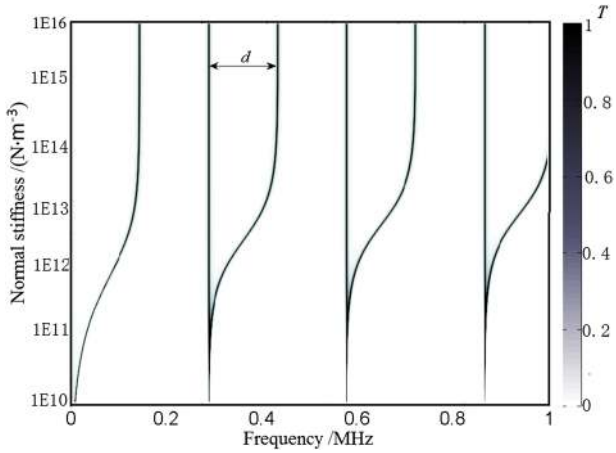

FIG. 3. The relationship between transmission coefficient and certain combinations K_N and frequency (θ_i=0°).

towards higher frequency as the value of K_N increase. This result indicates it is in accordance with the theory of 'peak drift'. If the K_N are more than 1×10^{15} N·m^{-3}, all of these peaks would stabilize nearly. By calculations and analysis, it is found that these peaks are available when the thicknesses of the tested materials are an integral multiple of a half wavelength. This result from the simulation is completely in accordance with the half-wave resonance theory.[34]

The symbol '*d*' marked in Fig. 3 denotes the shift distance of the transmission peak. The magnitude of *d* can be employed to indicate the sensitivity of the transmission peak with respect to K_N. The more shift distance means the more sensitivity. In order to find the maximum of shift distance at different incident angles, the lines labeled A_2 in Fig. 2(a) and Fig. 2(c) have been abstracted (note: if the lines labeled A_3 or A_4 was abstracted to analyze, the same rules can be emerged). According to the previous illustration, only the incident angles from 8° to 15° are chosen as the optimization parameter.

The shift distance against the incident angle is shown in Fig. 4. From the figure, the shift distance decrease to a minimum value and then increase with the increase of the incident angle. Increasing the incident angle, in the range greater than 10° and less than the second critical angle, can contribute to promoting the sensitivity for measuring the normal stiffness (K_N). However, if the incident angle is more than 15°, the resonant peaks are seldom and even hard to observe in Fig. 2. Therefore, incident angle 15° is considered to be the optimal angle to measure the normal stiffness K_N. Meanwhile, when the angle of incidence is at 13.27°, the shift distance is equal to the distance from the normal incidence.

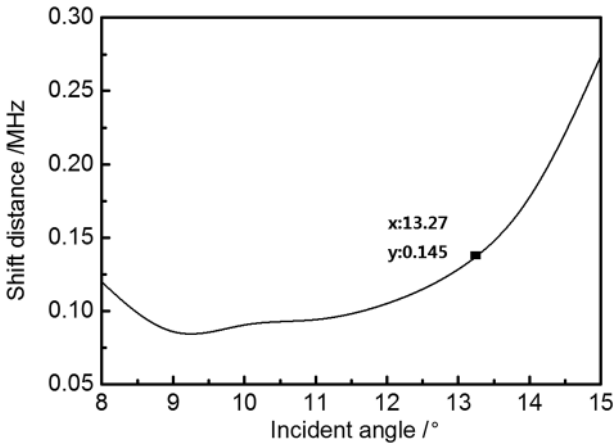

FIG. 4. The shift distance versus the incident angle.

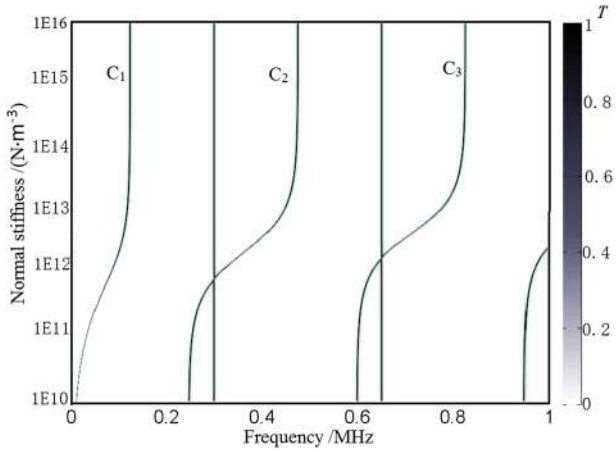

FIG. 5. The relationship between transmission coefficient and certain combinations K_N and frequency (θ_i=15° and K_T=10^{20} N·m^{-3}).

According to the previous analysis, Fig. 5 shows the shift of the transmission peaks with respect to the normal stiffness in different frequency, as the incident angle is 15°. In order to describe in the following text conveniently, these curves in Fig. 5 have been labeled 'C_n' (n=1, 2, 3). The shift pattern of transmission peaks is similar to that shown in Fig. 3, but its amplitude is larger. The sensitivity of resonant peaks in different frequency has varied with the variation of the normal stiffness K_N. It is significant to present this shift regularity for choosing an air-coupled transducer with an appropriate basic frequency and its frequency band.

The variable W_N is introduced to denote the slope of the curve labeled 'C_n' in Fig. 5. Since these slopes could describe the changing speed of transmission peaks with the change of the normal stiffness K_N, the W_N can be considered to characterize the relative sensitivity of resonant peaks to the normal stiffness. The W_N against normal stiffness K_N is shown in Fig. 6. It can be seen the amplitude of C_1 is maximum when the normal stiffness is less than 1×10^{11}N·m^{-3}. Nevertheless the amplitude of C_3 is maximum when the normal stiffness is more than 6×10^{12} N·m^{-3}. It is so concluded that the higher frequency peaks are 'later shift' than lower frequency peaks. The test frequency can be determined as needed in terms of changing regulation in Fig. 6.

B. Optimization of the parameters for measuring the transverse stiffness

For choosing the optimal parameters to measure the transverse stiffness K_T, the research procedure, which is the same to that of previous involving the normal stiffness, is carried out. Firstly, the

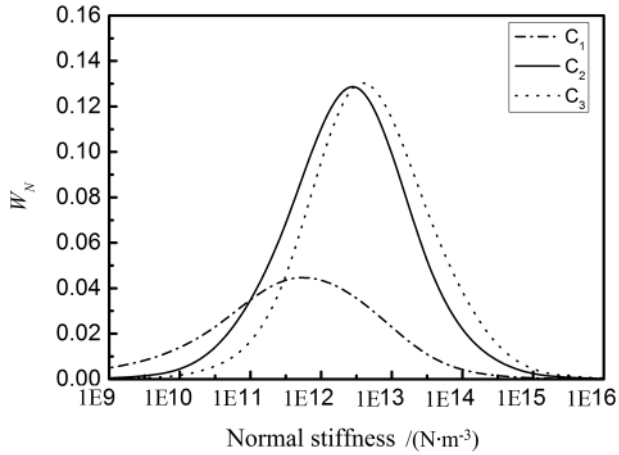

FIG. 6. The W_N versus the normal stiffness K_N.

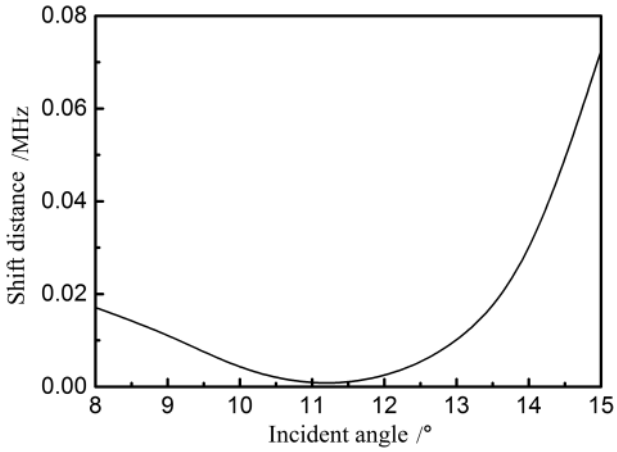

FIG. 7. The shift distance versus the incident angle.

curve labeled 'B_1' in Fig. 2 has been abstracted, and then the shift distance '*d*' of the transmission peak due to the influence of transverse stiffness at the different incident angle is illustrated in Fig. 7. It can be observed the shift distance also decreases to a minimum value before increases with the

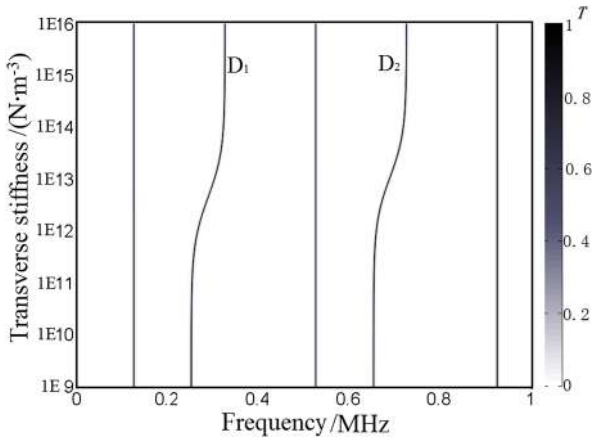

FIG. 8. The relationship between transmission coefficient and certain combinations K_T and frequency (θ_i=15° and K_N =10^{20} N·m^{-3}).

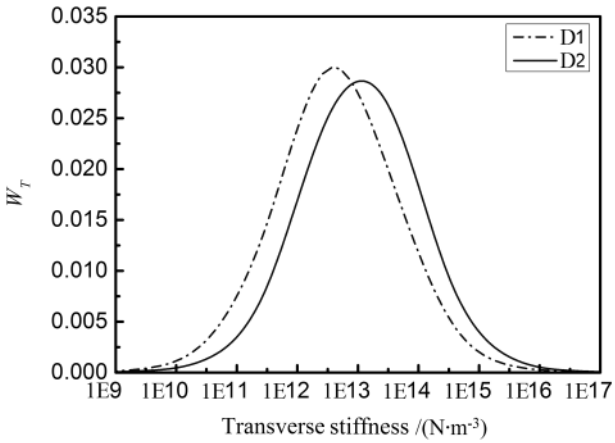

FIG. 9. The W_N versus transverse stiffness K_T.

increasing of the incident angle. Subsequently, the shift process curves that the resonant peaks change with the change of transverse stiffness at the incident angle 15° are shown in Fig. 8.

Similarly, these curves in Fig. 8 have been labeled 'D_n' (n=1, 2) for describing convenient in the following text, and the variable W_T has been also introduced to denote the slope of the curve labeled 'D_n' in Fig. 8. The slope of the peaks shift curve (W_T) in Fig. 8 against the transverse stiffness (K_T) is shown in Fig. 9. The shift of the resonant peak in the high frequency lags behind that in the low frequency from this figure. According to this analysis, the better test frequency can be chosen to measure the transverse stiffness.

IV. EXPERIMENTAL

A. Experimental setup

The ultrasonic system is employed to measure the weak bond interfacial stiffness illustrated in Fig. 10. A pair of air-coupled transducers are fixed on opposite sides of the adhesive composite material, the above transducer for transmitting and the below one for receiving. The transmitters are provided by Transducer Ltd in Japan. The adhesive specimens install on rotating table which can be adjusted the angle freely for experiment.

Ultrasonic pulses generated by the ultrasonic pulser/receiver propagate through pulser transducer, the air, the adhesive specimen, and finally are received by the receiver transducer. The receive signals are amplified by the receiver power amplifier which flat gain is 60 dB transmitted in turn to ultrasonic pulser/receiver, A/D acquisition card and personal computer.

B. Specimen preparation

Ten composite material plates (100mm×100mm×4.7mm) are fabricated by Minyi Co., LTD. The properties of the composite material plates, which include p-wave velocity, s-wave velocity and density have measured by an experimental method. The experiment results shown that these properties are uniform in different place and different directions, so these materials are regarded as isotropic materials. These materials have been ensured by ultrasonic c-scan method that there are no gross imperfections. The composite materials properties are listed in Table I.

Every two plates are bonded by a two part epoxy adhesive. The proportion of these two parts is 1:1, which is recommended by the manufacturer. Because the stressed force and temperature have an influence on the bond property of the epoxy adhesive, the conditions have almost been maintained consistency during the all experiment. The purpose that a group consisting of five experiment results under the same condition are chosen is to reduce the measurement error. The tested materials are pressured by heavy stuffs all the time, except the measuring process. The thickness of the adhesive

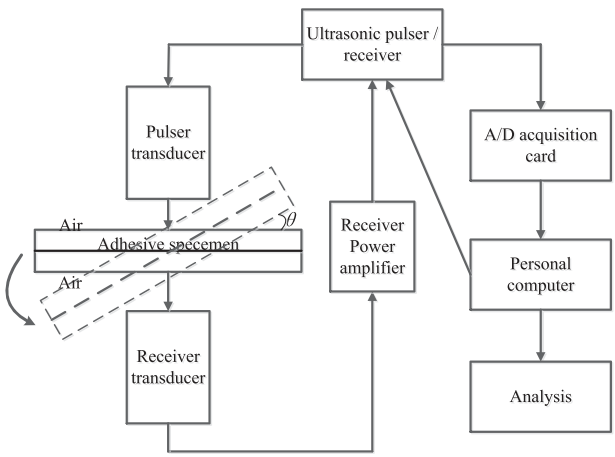

FIG. 10. Schematic diagram of the experimental setup used to measure the weak bonding interfacial stiffness.

layer measured by vernier calipers is approximately 0.02mm, so the thickness and attenuation are negligible.

Along with the increase of the bonding time which achieves the maximum after 12 hours, there has come an increase in the bonding strength of two part epoxy adhesive. Therefore, the specimens are taken a measurement per hour before 12 hours and the experimental data are recorded by computer. The time domain signals are transformed into the frequency domain using Fast Fourier Transform (FFT). By contrasting the two peaks from the experiment and numerical simulation, the interfacial stiffness can be obtained.

V. EXPERIMENTAL RESULTS AND DISCUSS

In the light of the previous analysis, choosing a proper transducer with the basic frequency and incident angle is a key part of achieving more accurate result. The range of stiffness which is about $1\times10^{14}\mathrm{N\cdot m^{-3}}$ has been published in the previous paper.[35] The transducer with the basic frequency 800 kHz is chosen and the incident angle of 15° is applied for experiments, because normal stiffness K_N and the transverse stiffness K_T change simultaneously actually, all the peaks will shift. It is difficult to distinguish which peaks have been affected by the K_N and which by K_T. As a result, the experiments of normal incidence are implemented to measure the normal stiffness, and then the resonant peaks influenced by transverse stiffness can be confirmed. Since the standard deviation of the transducer frequency is about 64 kHz, the frequency range of 0.5 MHz to 1MHz has been considered valid. The sampling frequency is 10 MHz and the voltage amplitude is 480 V. The time signals can be obtained from these experiments. It is necessary to transform these signals into frequency domain using Fourier Transform. The resolution of the frequency domain signal in the experiment is 1 kHz.

To evaluate frequency sensitiveness to stiffness, it is necessary to measure specimens at different bonding time. The frequency domain from normal incidence is shown in Fig. 11, in which the bonding time is 1 hour and 10 hours, respectively. Due to the transmission signal was amplified by the receiver power amplifier, the voltage amplitude from the receiver transducer which only represent the relative size was normalized. From the figure, the peaks in the frequency of 0.57 MHz and 0.86 MHz are almost stable on condition of the bonding time from 1 hour to 10 hours. However, the frequency in the midst of these two peaks moves towards higher frequency area sharply with the increase of the bonding time in comparison. Firstly, the results from the experiment match exactly with the previous numerical calculation results. Furthermore, by comparing the position of the midst peak in the experiment with theoretical positions in Fig. 3, the normal stiffness can be estimated.

The frequency spectrums at the incident angle15° and the different bonding times (1 hour and 10 hours) are shown in Fig. 12. It can be seen that both peaks move towards higher frequency area as the bonding time goes from 1 hour to 10 hours. In terms of the normal interface stiffness from measurement results of the normal incidence, the second peak as shown in Fig. 12 is relevant to the

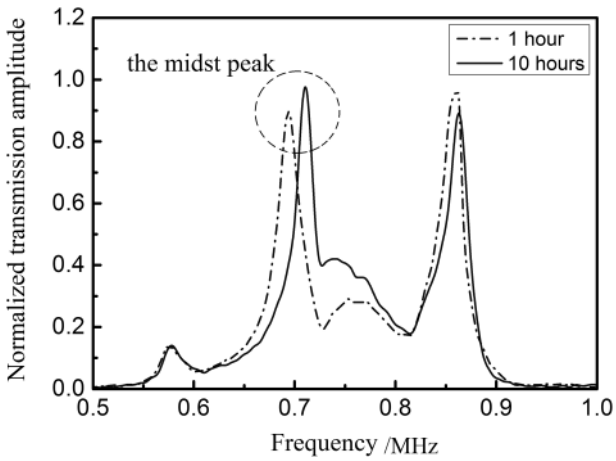

FIG. 11. The frequency spectrum from normal incidence.

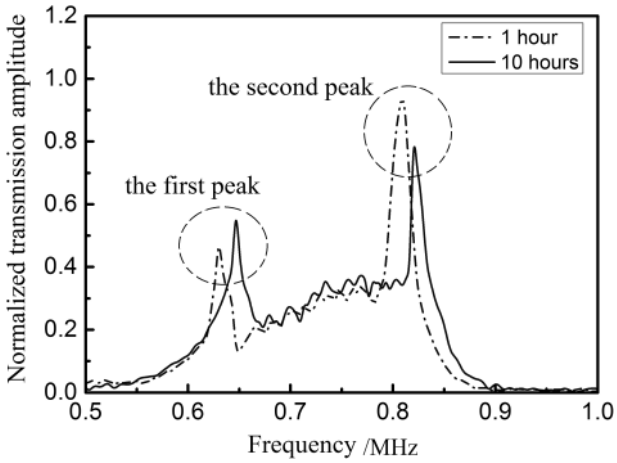

FIG. 12. The frequency domain signal from 15° incident angle.

normal stiffness, and the first peak is relevant to the transverse stiffness. The shift distance of this peak is greater than that from the normal incidence.

There are five experiment results under the same bonding time. By statisticing and analyzing these data, the mean and the standard deviation which are showed by the error bars in Fig. 13 can be

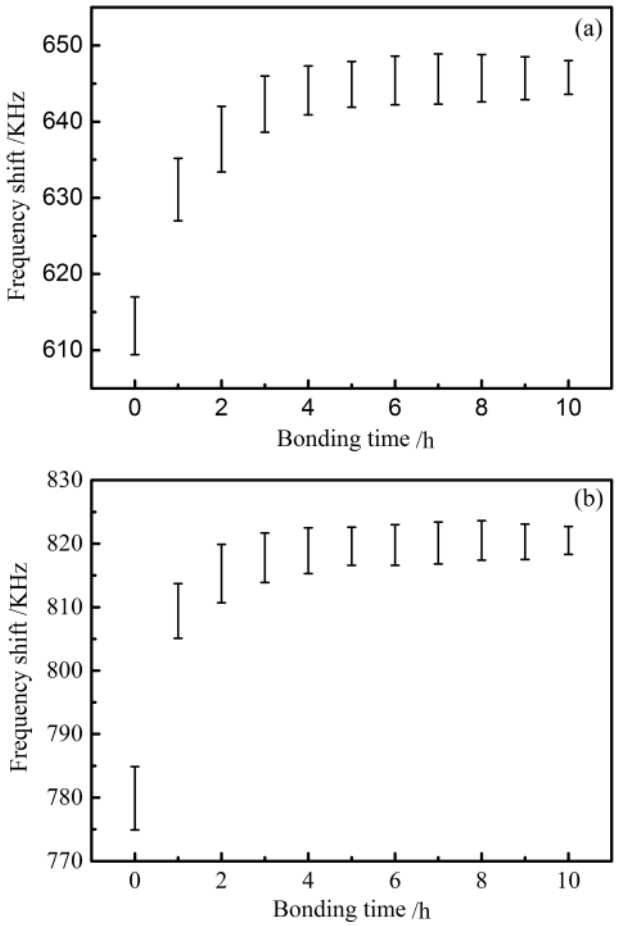

FIG. 13. The frequency of peaks versus the bonding time (a) the first peak; (b) the second peak.

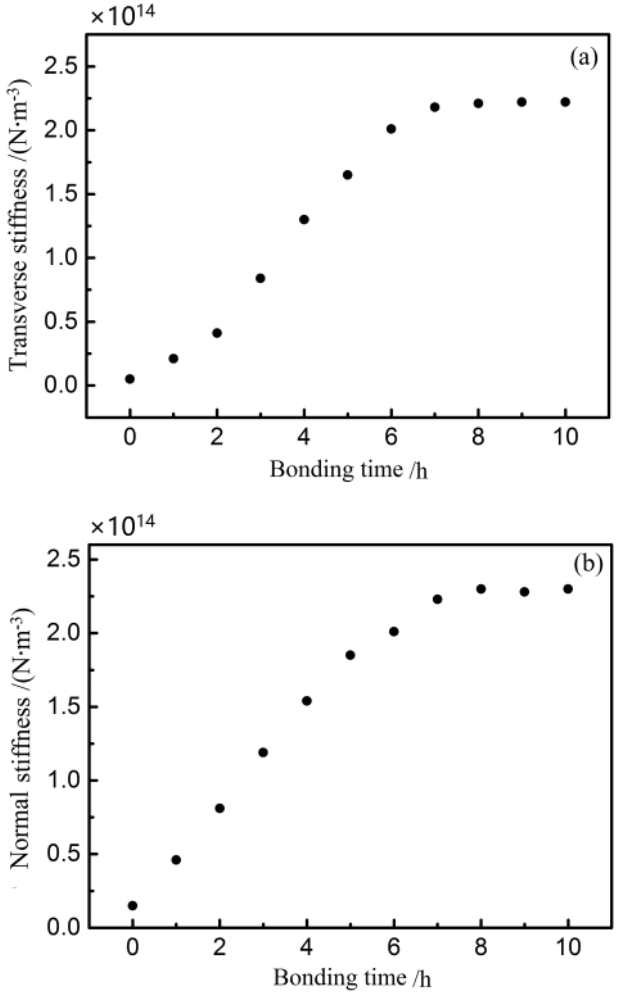

FIG. 14. The interfacial stiffness versus the bonding time: (a) transverse stiffness; (b) normal stiffness.

obtained in ervey bonding time. Figure 13(a) and (b) illustrate the relationship between the frequency of peaks and the bonding time. Fig. 13(a) depicts the frequency of the first peak and Fig. 13(b) depicts the frequency of the second peak. The frequency moves towards higher frequency area with the increasing of the bonding time. The movement velocity is too quickly at the first, and then slows later. Finally, frequency of the peak almost does not move after 8 hours. The standard errors of frequency decrease with the increasing of the bonding time.

Figure 5 and Figure 8 show the simulation results which are obtained by calculated by Eq. (7), when the incident angle is 15°, while Fig. 13 shows the experiment results which is also from 15°incident angle. The normal stiffness can be obtained by comparing the mean of the peak positions in Fig. 13 (b) with the line C_3 in fig. 5. Similarly, the transverse stiffness be obtained by comparing the mean of the peak positions in Fig. 13 (a) with the line D_2 in Fig. 8. The interfacial stiffness including the transverse and the normal stiffness against the bonding time are shown in Fig. 14 (a) and Fig. 14 (b), respectively. According to these results, the bonding strength at any time can be obtained. Using this method can evaluate the curing velocity of adhesive and ultimate bonding strength.

VI. CONCLUSION

Through theoretically analyzing ultrasonic propagating characteristics in double-layer plate bonding structure, it has demonstrated that some of the transmission peaks are only related to the

normal interfacial stiffness (K_N) and others to the transverse interfacial stiffness (K_T). All these peaks shift towards higher frequency with the increasing interfacial stiffness, but the sensitivity is different due to the variation in the incidence angle and testing frequency. The higher frequency peaks are 'later shift' than lower frequency peaks. These rules provide relevant the theoretical basis for optimizing inspection parameters. According to the actual situation, it can improve the sensitivity through choosing the ultrasonic testing parameters. In this paper, the interfacial stiffness of double-layer adhesive composite plate, which changes with the bonding time, is accurately measured by using air-coupled ultrasound.

ACKNOWLEDGMENTS

This research is supported by the National Natural Science Foundation of China (Grant No. 51565020 and No. 51305184) and the Natural Science Foundation of Jiangxi Province, China (Grant No. 20171BAB206032).

APPENDIX

The element of matrix A are as follows

$A_{11} = k_a cos\theta_i; A_{12} = k_{L(1)} cos\theta_{L(1)}; A_{13} = -A_{12}; A_{14} = k_{T(1)} \sin\theta_{T(1)}; A_{15} = A_{14};$

$A_{21} = \rho_a\omega^2; A_{22} = 2\mu_1 k_{L(1)} \sin\theta_{L(1)} - \rho_1\omega^2; A_{23} = A_{22}; A_{24} = -\mu_1 k_{T(1)}^2 \sin(2\theta_{T(1)}); A_{25} = -A_{24};$

$A_{32} = -k_{L(1)}^2 \sin(2\theta_{L(1)}); A_{33} = -A_{32}; A_{34} = k_{T(1)}^2 \cos(2\theta_{T(1)}); A_{35} = A_{34};$

$A_{42} = -k_{L(1)} \sin\theta_{L(1)} K_T e^{L_1}; A_{43} = -k_{L(1)} \sin\theta_{L(1)} K_T e^{-L_1}; A_{44} = k_{T(1)} \cos\theta_{T(1)} K_T e^{T_1};$

$A_{45} = -k_{T(1)} \cos\theta_{T(1)} K_T e^{-T_1}; A_{46} = k_{L(2)} \sin\theta_{L(2)} K_T + k_{L(2)}^2 \sin(2\theta_{L(2)});$

$A_{47} = k_{L(2)} \sin\theta_{L(2)} K_T - k_{L(2)}^2 \sin(2\theta_{L(2)});$

$A_{48} = -k_{T(2)} \cos\theta_{T(2)} K_T - (k_{T(2)} \cos\theta_{T(2)})^2 + (k_{T(2)} \cos\theta_{T(2)})^2;$

$A_{49} = k_{T(2)} \cos\theta_{T(2)} K_T - (k_{T(2)} \cos\theta_{T(2)})^2 + (k_{T(2)} \cos\theta_{T(2)})^2;$

$A_{52} = k_{L(2)} \cos\theta_{L(2)} K_N e^{L_1}; A_{53} = -k_{L(2)} \cos\theta_{L(2)} K_N e^{-L_1}; A_{54} = k_{T(1)} \sin\theta_{T(1)} K_N e^{T_1};$

$A_{55} = k_{T(1)} \sin\theta_{T(1)} K_N e^{-T_1}; A_{56} = -k_{L(2)} \cos\theta_{L(2)} K_N - 2\mu_2 (k_{L(2)} \sin\theta_{L(2)})^2 + \rho_2\omega^2;$

$A_{57} = k_{L(2)} \cos\theta_{L(2)} K_N - 2\mu_2 (k_{L(2)} \sin\theta_{L(2)})^2 + \rho_2\omega^2; A_{58} = -k_{T(2)} \sin\theta_{T(2)} K_N + \mu_2 k_{T(2)}^2 \sin(2\theta_{T(2)});$

$A_{59} = -k_{T(2)} \sin\theta_{T(2)} K_N - \mu_2 k_{T(2)}^2 \sin(2\theta_{T(2)});$

$A_{62} = -k_{L(1)}^2 \sin(2\theta_{L(1)}) e^{L_1}; A_{63} = k_{L(1)}^2 \sin(2\theta_{L(1)}) e^{-L_1}; A_{64} = k_{T(1)}^2 \cos(2\theta_{T(1)}) e^{T_1};$

$A_{65} = k_{T(1)}^2 \cos(2\theta_{T(1)}) e^{-T_1}; A_{66} = k_{L(2)}^2 \sin(2\theta_{L(2)}); A_{67} = -k_{L(2)}^2 \sin(2\theta_{L(2)}); A_{68} = -k_{T(2)}^2 \cos(2\theta_{T(2)});$

$A_{69} = A_{68};$

$A_{72} = (2\mu_1 k_{L(1)} \sin\theta_{L(1)} - \rho_1\omega^2) e^{L_1}; A_{73} = (2\mu_1 k_{L(1)} \sin\theta_{L(1)} - \rho_1\omega^2) e^{-L_1};$

$A_{74} = -\mu_1 k_{T(1)}^2 \sin(2\theta_{T(1)}) e^{T_1}; A_{75} = \mu_1 k_{T(1)}^2 \sin(2\theta_{T(1)}) e^{-T_1}; A_{76} = 2\mu_2 k_{L(2)} \sin\theta_{L(2)} - \rho_2\omega^2;$

$A_{77} = A_{76}; A_{78} = \mu_2 k_{T(2)}^2 \sin(2\theta_{T(2)}); A_{79} = -A_{78};$

$A_{86} = -k_{L(2)} cos\theta_{L(2)} e^{L_2}; A_{87} = k_{L(2)} cos\theta_{L(2)} e^{-L_2}; A_{88} = k_{T(2)} \sin\theta_{T(2)} e^{T_2}; A_{89} = k_{T(2)} \sin\theta_{T(2)} e^{-T_2};$

$A_{8(10)} = k_a cos\theta_r;$

$A_{96} = 2\mu_2 k_{L(2)} \sin\theta_{L(2)} e^{L_2}; A_{97} = 2\mu_2 k_{L(2)} \sin\theta_{L(2)} e^{-L_2}; A_{98} = -\mu_2 k_{T(2)}^2 \sin(2\theta_{T(2)}) e^{T_2};$

$A_{99} = \mu_2 k_{T(2)}^2 \sin(2\theta_{T(2)}) e^{-T_2}; A_{9(10)} = \rho_a\omega^2;$

$A_{(10)6} = -k_{L(2)}^2 \sin(2\theta_{L(2)}) e^{L_2}; A_{(10)7} = k_{L(2)}^2 \sin(2\theta_{L(2)}) e^{-L_2}; A_{(10)8} = k_{T(2)}^2 \cos(2\theta_{T(2)}) e^{T_2};$

$A_{(10)9} = k_{T(2)}^2 \cos(2\theta_{T(2)}) e^{-T_2};$

The rest elements are zero.

[1] A. Baker, D. Bitton, and W. JOHN, "Development of a proof test for through-life monitoring of bond integrity in adhesively bonded repairs to aircraft structure," International Journal of Adhesion and Adhesives **36**, 65–76 (2012).
[2] R. J. Lord, "In-service nondestructive inspection of fighter and attack aircraft," Materials Evaluation **43**, 733–739 (1985).
[3] R. D. Adams and B. W. Drinkwater, "Nondestructive testing of adhesively-bonded joints," NDT&E International **30**(2), 93–98 (1997).
[4] Y. Binfeng, L. Feilu, Z. Yuhua *et al.*, "Quantification and classification of cracks in aircraft multi-layered structure," Chinese Journal of Mechanical Engineering **42**(2), 63–67 (2006).
[5] D. W. Schindel, "Air-coupled ultrasonic measurements of adhesively bonded multi-layer structures," Ultrasonics **37**, 185–200 (1999).
[6] P. Cawley, "The rapid non-destructive inspection of large composite structures," Composites **25**(5), 351–357 (1994).
[7] X. Wu and K. Peters, "Non-destructive inspection of adhesively bonded joints using amplitude modulated thermography," Experimental Mechanics **55**(8), 1–17 (2015).
[8] P. Mylavarapu and E. Woldesenbet, "Non-destructive characterization of bondlines in composite adhesive joints," Journal of Adhesion Science and Technology **20**(7), 647–660 (2006).
[9] R. J. Pryputniewicz, "Quantitative non-destructive testing of adhesive joints," 33rd Annual Techincal Symposium. International Society for Optics and Photonics, 1990:440–445.
[10] P. Boinard, R. A. Pethrick, W. M. Banks *et al.*, "Non-destructive evaluation of adhesively bonded composite structures using high frequency dielectric spectroscopy," Journal of Materials Science **35**(6), 1331–1337 (2000).
[11] V. Nigrelli, "Detection of disbond in multi-layer structures by laser-based ultrasonic technique," Journal of Adhesion **84**(10), 811–829 (2008).
[12] Z. Yang, W. Zhang, C. Wu *et al.*, "Infrared thermography applied to evaluate adhesive quality of missile motor shell," Chinese Journal of Scientific Instrument (2010).
[13] X. U. Meng, X. U. Yan-Lin, Z. Y. Wang *et al.*, "Ultrasonic testing techniques and progress of adhesive structure," Machinery (2007).
[14] M. Korzeniowski, T. Piwowarczyk, and R. G. Maev, "Application of ultrasonic method for quality evaluation of adhesive layers," Archives of Civil & Mechanical Engineering **14**(4), 661–670 (2014).
[15] M. Castaings, E. Siryabe, M. Renier *et al.*, "Ultrasonic characterization of cohesive and adhesive properties of adhesive bonds," Journal of the Acoustical Society of America **138**(3), 1766–1766 (2015).
[16] P. Mylavarapu and E. Woldesenbet, "Non-destructive characterization of bondlines in composite adhesive joints," Journal of Adhesion Science and Technology **20**(7), 647–660 (2006).
[17] N. Bochud, Q. Vallet, J. G. Minonzio *et al.*, "Predicting bone strength with ultrasonic guided waves," Scientific Reports **7**, 43628 (2017).
[18] S. Mezil, J. Laurent, D. Royer *et al.*, "Non contact probing of interfacial stiffnesses between two plates by zero-group velocity Lamb modes," Applied Physics Letters **105**(2), 021605–021605-4 (2014).
[19] R. E. Challis, U. Bork, and P. C. D. Todd, "Ultrasonic NDE of adhered of T-joints using Lamb waves and intelligent signal processing," Ultrasonics **34**, 455–9 (1996).
[20] M. J. S. Lowe, R. E. Challis, and C. W. Chan, "The transmission of Lamb waves across adhesively bonded lap joints," J Acoust Soc Am **107**(3), 1333–1345 (2000).
[21] S. Mustapha, L. Ye, D. Wan *et al.*, "Assessment of debonding in sandwich CF/EP composite beams using A_0 Lamb wave at low frequency," Composite Structures **93**, 483–491 (2011).
[22] H. G. Tattersall, "The ultrasonic pulse-echo technique as applied to adhesion testing," Journal of Physics D Applied Physics **6**(7), 819–832 (2002).
[23] R. E. Challis, R. J. Freemantle, G. P. Wilkinson *et al.*, "Compression wave NDE of adhered metal lap joints: Uncertainties and echo feature extraction," Ultrasonics **34**, 455–9 (1996).
[24] C. M. Paralusz, "Internal reflection spectroscopy applied to the analysis of adhesive tapes," Journal of Colloid & Interface Science **47**(3), 719–746 (1974).
[25] C. Junjie, L. Chao, and O. Yukio, "Research the principle and application of non-contact air coupling ultrasonic testing," Nondestructive Inspection **37**(4) (2013).
[26] Z. Zhenggan and W. Dong, "Progress of air-coupled ultrasonic non-destructive testing technology," Chinese Journal of Mechanical Engineering **44**(6) (2008).
[27] D. W. Schindel, D. S. Forsyth, D. A. Hutchins *et al.*, "Air-coupled ultrasonic NDE of bonded aluminum lap joints," Ultrasonics **35**, 1–6 (1997).
[28] F. Windels and O. Leroy, "Air-coupled ultrasonic testing of diffusion bonds," Ultrasonics **40**(1-8), 171–176 (2002).
[29] S. J. Sanabria, R. Furrer, J. Neuenschwander *et al.*, "Novel slanted incidence air-coupled ultrasound method for delamination assessment in individual bonding planes of structural multi-layered glued timber laminates," Ultrasonics **53**(7), 1309–1324 (2013).
[30] N. M. Newmark, C. P. Siess, and I. M. Viest, "Tests and analysis of composite beams with incomplete interaction," Proc. Soc. Exp. Stress Anal. **9**(1), 75–92 (1951).
[31] L. Brekhoviskikh and O. Godin, *Acoustics of layered media*, Berlin: Springer Verlag, 1990.
[32] J. L. Rose, *Ultrasonic waves in solid media* (Cambridge University Press, 1999).
[33] W. Xingguo, W. Wenlin, C. Zhenglin *et al.*, "Testing stiffness coefficient of coating interface based on ultrasonic numerical simulation," Acta Materiae Compositae Sinica **34** (2017).
[34] A. I. Lavrentyev and S. I. Rokhlin, "Ultrasonic spectroscopy of imperfect contact interfaces between a layer and two solids," Journal of the Acoustical Society of America **103**(103), 657–664 (1998).
[35] A. Zhiwu, W. Xiaomin, M. Jie *et al.*, "Low-frequency characteristic of ultrasound reflection spectrum from adhesively bonded aluminum plates," Applied Acoustics **28**(3), 190–194 (2009).